Correlation-Driven 3d Heavy Fermion Behavior in LiV_2O_4

Minyinan Lei(雷珉毅楠)[1], Zhihui Chen(陈志辉)[1], Haitao Wang(王海涛)[1], Yu Fan(樊钰)[1], Nan Guo(郭楠)[1], Tianxing Jiang(姜天星)[1], Yanwei Cao(曹彦伟)[2], Tong Zhang(张童)[1,3,4], Rui Peng(彭瑞)[1,4*], and Haichao Xu(徐海超)[1,4*]

[1]*Laboratory of Advanced Materials, State Key Laboratory of Surface Physics, and Department of Physics, Fudan University, Shanghai 200438, China*
[2]*Ningbo Institute of Materials Technology and Engineering, Chinese Academy of Sciences, Ningbo 315201, China*
[3]*Hefei National Laboratory, Hefei 230088, China*
[4]*Shanghai Research Center for Quantum Sciences, Shanghai 201315, China*

(Received 7 August 2025; accepted manuscript online 5 September 2025)

LiV_2O_4 is a spinel-structured compound that stands out as the first known 3d-electron system exhibiting typical heavy fermion behavior. A central question is how such strong mass renormalization emerges in the absence of f-electrons. In this work, we investigate the three-dimensional electronic structure of LiV_2O_4 thin films using angle-resolved photoemission spectroscopy. We identify that an electron-like flat band is derived from a_{1g} orbitals, along with a highly dispersive e'_g band strongly coupled with phonons. The overall agreement with dynamical mean-field theory calculations highlights the essential role of inter-orbital Hund's coupling in reducing the a_{1g} bandwidth to 25 meV, approaching a Mott state. Notably, we find that heavy-fermion behavior arises from additional renormalization at the a_{1g} band near the Fermi level, likely driven by many-body interactions at energy scales down to a few meV and potentially linked to geometric frustration inherent to the spinel lattice. These results provide crucial insights into the origin of the heavy fermion behavior in 3d-electron systems.

DOI: 10.1088/0256-307X/42/10/100710 CSTR: 32039.14.0256-307X.42.10.100710

1. Introduction. Heavy fermion materials have long attracted interest in condensed matter physics due to the correlation-driven exotic quantum states, such as unconventional superconductivity and complex magnetic orders.[1–6] In typical heavy fermion systems, such as $CeCoIn_5$[7] and $CeCu_2Si_2$,[8] strong electronic correlations have typically been attributed to the hybridization between localized f-orbital electrons and itinerant conduction electrons.[9] This hybridization leads to a substantial enhancement of the quasiparticle effective mass, with values ranging from 100 to 1000 times the free electron mass (m_e), as inferred from specific heat measurements.[4,10] Remarkably, the 3d transition-metal oxide LiV_2O_4 exhibits a similarly large Sommerfeld coefficient ($\gamma \simeq 0.42\,\mathrm{J/mol{\cdot}K^2}$), corresponding to an effective mass of approximately $180m_e$. This value rivals those found in typical f-electron heavy fermion compounds, despite the absence of f-electrons in LiV_2O_4,[11,12] which presents a longstanding puzzle regarding the microscopic origin of its heavy fermion behavior.

Various scenarios have been proposed to explain the microscopic origin of heavy fermion behavior in LiV_2O_4. In the spinel structure of this compound, the crystal field splits the V 3d t_{2g} orbitals into a narrow a_{1g} band and broader e'_g bands.[13,14] One proposed mechanism involves hybridization between the more localized a_{1g} states and the itinerant e'_g states, leading to mass renormalization analogous to the c–f hybridization.[13] Alternatively, dynamical mean-field theory (DMFT) calculations suggest that LiV_2O_4 is best described as a lightly hole-doped Mott insulator in the a_{1g} orbital.[15] In this picture, the enhanced quasiparticle mass originates not from hybridization, but from the proximity to a Mott–Hubbard transition. Hund's coupling has also been identified as a key factor in driving orbital differentiation and pushing the system toward an orbital-selective Mott–Hubbard transition.[16] The geometrical frustration inherent to the spinel lattice [Fig. 1(a)], where V atoms occupy a pyrochlore sublattice, can promote strong spin fluctuations, which may additionally contribute to the heavy effective mass.[17,18] Despite these theoretical proposals, a direct experimental determination of the three-dimensional electronic structure near the Fermi level remains lacking. Such information is crucial for elucidating the mechanisms underlying heavy fermion behavior in LiV_2O_4. Previous photoemission studies have been limited to angle-integrated spectra, partly due to the difficulty of preparing high-quality surfaces in this three-dimensional correlated oxide.[10]

Here, we reveal the three-dimensional electronic structure of LiV_2O_4 by combining film growth with angle-resolved photoemission spectroscopy (ARPES). Our experimental results show overall agreement with DMFT calculations, supporting the pivotal role of inter-orbital

*Corresponding authors. Email: pengrui@fudan.edu.cn; xuhaichao@fudan.edu.cn
© 2025 Chinese Physical Society and IOP Publishing Ltd. All rights, including for text and data mining, AI training, and similar technologies, are reserved.

Hund's coupling in driving the a_{1g} orbitals towards a Mott state. The measured dispersion of the flat a_{1g} band deviates from a parabolic form and instead indicates an additional renormalization on a scale of a few meV near the Fermi level. This additional renormalization suggests that the coupling between electrons and low-energy excitations on the few-meV scale, possibly arising from geometric frustration, also plays important roles in the formation of the heavy fermion state in LiV_2O_4.

2. Results. Atomically flat LiV_2O_4 thin films were grown on Nb:$SrTiO_3$(111) substrates for ARPES studies [Fig. 1(b)]. We fabricated films with a thickness of 72 nm by ablating ceramic targets with a KrF excimer laser ($\lambda =$ 248 nm, repetition rate 10 Hz, fluence 0.6 J/cm^2) under an argon partial pressure of 1×10^{-4} mbar at a substrate temperature of 450 ℃. By optimizing the Li/V stoichiometry of the target, we successfully obtained high-quality LiV_2O_4 films. The x-ray diffraction results indicate that the films are fully relaxed, with lattice constants consistent with those of bulk LiV_2O_4 [see Section I of the Supplementary Materials (SM)]. The reflection high-energy electron diffraction (RHEED) pattern, shown in Fig. 1(c), reveals well-defined two-dimensional streaks, indicating a smooth and ordered surface. The low-energy electron diffraction (LEED) pattern, shown in Fig. 1(d), exhibits sharp spots consistent with the threefold symmetry of the LiV_2O_4 crystal along the [111] direction. Scanning tunneling microscopy (STM) images show an atomically smooth surface [Fig. 1(e)]. The details of the film growth process are provided in Section I of the SM. Temperature-dependent resistivity measurements were performed using a physical property measurement system [Fig. 1(f)]. At high temperatures, the films exhibit metallic behavior, with resistance decreasing upon cooling. As the temperature is lowered below $T^* \approx 30$ K, the differential resistivity undergoes a sudden change, which signifies a crossover into enhanced electronic coherence.[19,20] This characteristic temperature is consistent with previous resistivity measurements on bulk crystals[11,21] and high-quality thin films.[22,23]

Most ARPES data were collected at beamline 03U of the Shanghai Synchrotron Radiation Facility (SSRF). The data in Figs. 4(k) and 4(l) (discussed later) were obtained using the He lamp ARPES system at Fudan University, and the data in Section Ⅱ of the SM were collected at beamline QMSC of the Canadian Light Source. Both beamlines and the Fudan University ARPES system are equipped with Scienta DA30 electron analyzers. The overall energy resolution was set to 13 meV at Beamline 03U of the SSRF, 10 meV at the Fudan University He lamp ARPES system, and 20 meV at Beamline QMSC of the Canadian Light Source. The angular resolution was 0.1°. ARPES measurements were conducted under an ultrahigh vacuum of 5×10^{-11} mbar. At Fudan University, fresh films grown by pulsed laser deposition were transferred directly into the ARPES system via an interconnected ultrahigh-vacuum system. The thin films were transferred to SSRF for ARPES measurements in a vacuum suitcase (1×10^{-10} mbar), and the transfer was completed within

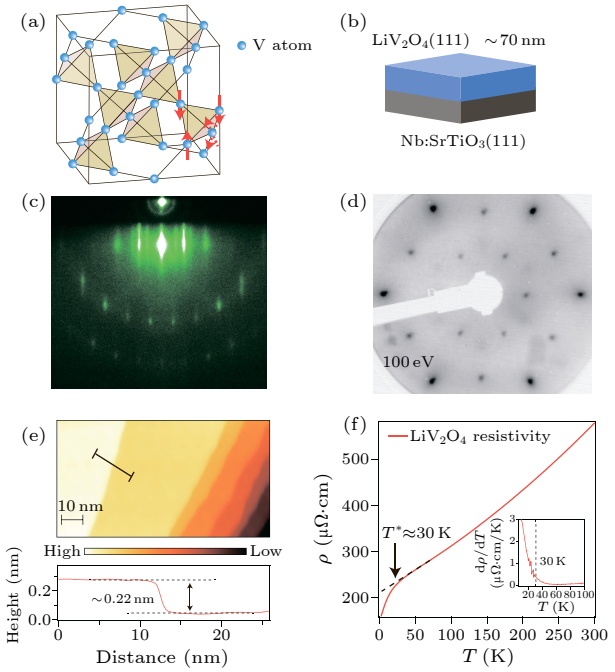

Fig. 1. (a) V sublattice in the LiV_2O_4 crystal. The arrows illustrate the geometric frustration in the corner-sharing V-based tetrahedra. (b) Schematic illustration of the LiV_2O_4 film grown on Nb:$SrTiO_3$ substrate. (c) RHEED pattern of the LiV_2O_4 thin film. Electron beam was incident along the [11$\bar{2}$] direction. (d) LEED pattern of the LiV_2O_4 thin film. (e) STM topographic image of the LiV_2O_4 thin film surface ($V_b = 1$ V and $I = 10$ pA). (f) Temperature-dependent resistivity of LiV_2O_4 thin film. The black dashed line represents the linear extrapolation from the temperature range of 50–100 K. T^* is defined as the temperature at which the resistance curve deviates from the linear extrapolation. The inset shows the derivative of resistance with respect to temperature.

12 hours. To minimize surface contamination, the samples were annealed at 300 ℃ for 30 minutes before measurements. A 30-nm-thick amorphous Se layer was deposited as a protective capping for transfer to Beamline QMSC at the Canadian Light Source. Before ARPES measurements, the samples were annealed in ultrahigh vacuum at 500 ℃ for 2 hours to remove the Se layer. The electronic structures of LiV_2O_4 obtained using different transfer methods are consistent with each other.

We measured the electronic structure of LiV_2O_4 by ARPES. The Fermi surface measured in the k_x–k_z plane exhibits strong intensity near the Γ point, located around $k_x = 0$ [Fig. 2(a)]. At $k_x = 2\pi/a$, the intensity near the Γ point is suppressed due to matrix element effects. Consequently, the intensity of the β band Fermi surface, which shows a k_z dispersion consistent with the periodicity of Brillouin zone, becomes dominant. In both the ΓKM and LWU planes, the photoemission intensity follows the threefold symmetry of the LiV_2O_4 crystal along the [111] direction [Figs. 2(b) and 2(c)].

Along the Γ–K cut, ARPES resolves two distinct bands: a weakly dispersive α band with relatively flat-band characteristics, and a highly dispersive β band [Fig. 2(e)]. Near the Fermi level, the flat α band intensity dominates, while the dispersion of the β band is obscured.

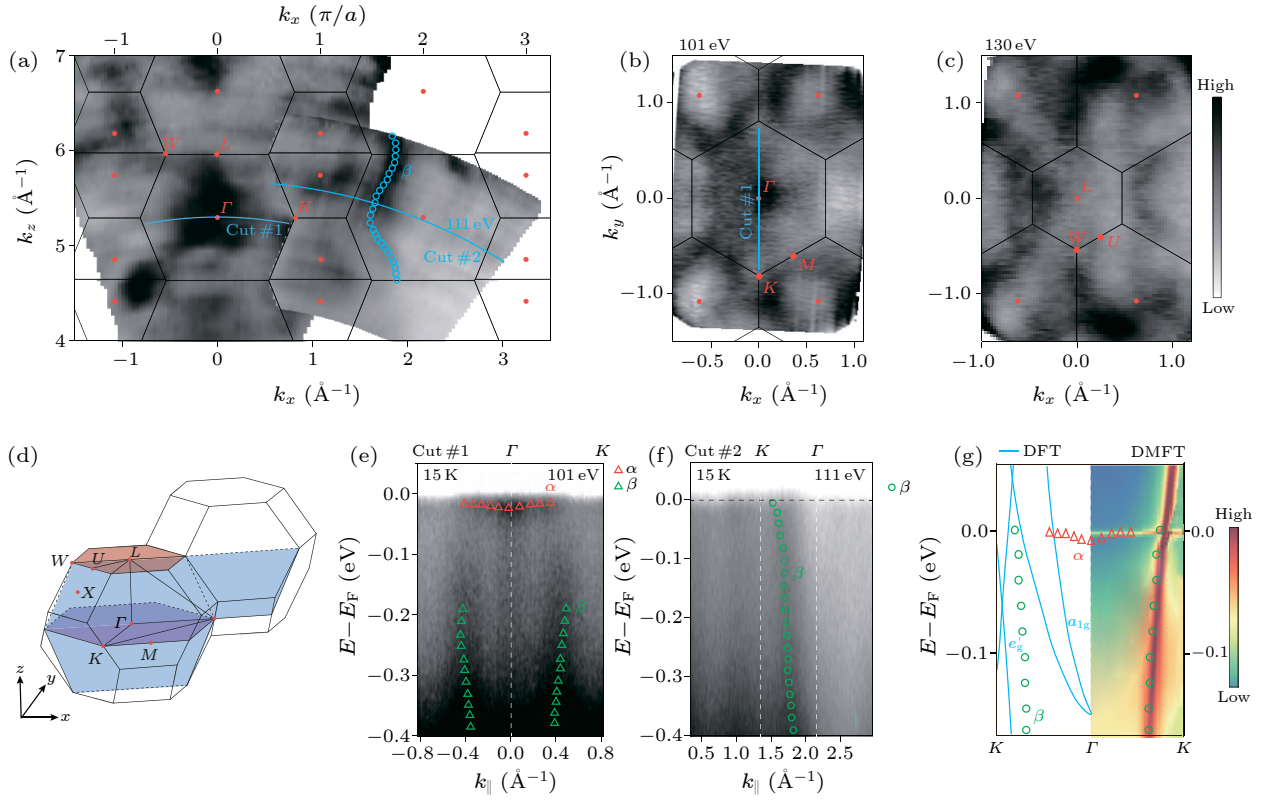

Fig. 2. (a) Photoemission intensity in the ΓLW plane, measured using 63 eV to 147 eV photons at 15 K, integrated over $E_F \pm 30$ meV. The inner potential was estimated as 15 eV. k_F's (blue open circles) were determined by the local maxima. (b) Photoemission intensity in the ΓKM plane integrated over $E_F \pm 60$ meV, collected with 101 eV photons at 15 K. (c) Photoemission intensity in the LWU plane integrated over $E_F \pm 30$ meV, collected with 130 eV photons at 15 K. (d) Sketch of the three-dimensional Brillouin zone. The momentum regions sampled in panels (a), (b), and (c) are indicated in blue, purple, and magenta, respectively. (e) Photoemission spectra along Γ–K direction (cut #1). The α and β bands are indicated by triangles determined from the local maxima of momentum distribution curves (MDCs) and energy distribution curves (EDCs). (f) Photoemission spectra of cut #2 illustrated in panel (a). The β band is indicated by circles determined from the local maxima of MDCs. (g) Comparison of DFT and DMFT calculations (adapted from Ref. [16]) with dispersions extracted from photoemission spectroscopy.

Along cut #2 [Fig. 2(f)], the α band is suppressed by matrix element effects, while the β band dispersion is better resolved. Figure 2(g) compares experimental band dispersions directly with theoretical calculations. The results show a deviation from the density functional theory (DFT) calculations but are consistent with DMFT calculations that incorporate electron–electron interactions and Hund's coupling.[16,24] Theoretical calculations indicate that the flat α band primarily originates from the a_{1g} orbital, while the dispersive β band is predominantly derived from the e'_g orbital.[16] The differences in orbital symmetry lead to different polarization sensitivity in ARPES spectra (see Section Ⅱ of the SM).

Higher-resolution spectra reveal a double kink feature in the β band [Fig. 3(a)]. The appearance of the kink in the band dispersion is a characteristic signature of boson–electron coupling. By fitting the band dispersion, we identify significant slope changes at binding energies of approximately 75 meV and 150 meV [Fig. 3(b)]. In the MDCs, we observe increases in peak widths at these two characteristic energies as well [Fig. 3(c)]. To further quantify these features, we extract the imaginary part of the quasiparticle self-energy ($\mathrm{Im}\Sigma$) from the full-width at half-maximum (FWHM) of the MDC peaks [Fig. 3(e)]. The real part ($\mathrm{Re}\Sigma$) is estimated from the difference between the experimentally observed dispersion and a bare band dispersion derived from the large-scale spectra.[25] Furthermore, $\mathrm{Re}\Sigma$ and $\mathrm{Im}\Sigma$ satisfy the Kramers–Kronig relation [Fig. 3(d)], which imposes additional constraints on the choice of the bare band dispersion. The band renormalization induced by electronic correlations can be estimated from the renormalized Fermi velocities, derived from the dispersion. The renormalized Fermi velocity $v_F = 1.19\,\mathrm{eV}\cdot\mathrm{Å}$ is obtained from the slope between the lower-energy kink and E_F, while the bare velocity v_F^0 is determined by the slope over a broader energy range [Fig. 3(b)]. We calculate a renormalization factor $Z = v_F^0/v_F = 3.4$ along the Γ–K direction.[26]

Phonon modes near 75 meV have previously been observed in optical reflectivity spectra of several spinel compounds, including $MgTi_2O_4$, $ZnCr_2O_4$, and $NiFe_2O_4$.[27,28] Takagi *et al.* suggested that comparable phonon energies are likely present in LiV_2O_4 due to its structural similarity to these materials.[20] If this is the case, the matching energy scale between the observed kink features and phonon modes suggests that electron–phonon

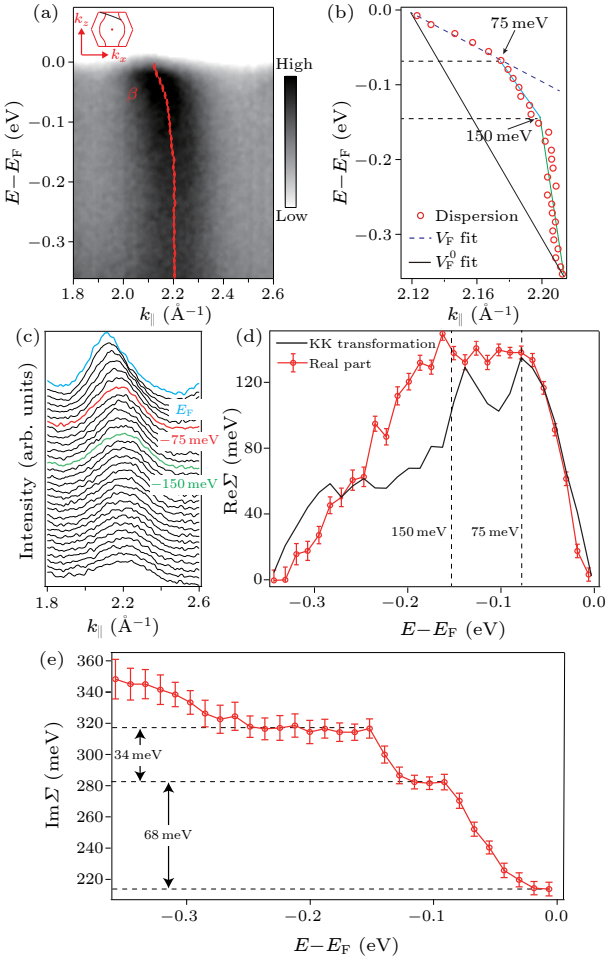

Fig. 3. (a) ARPES spectra were acquired using 136 eV photons at 15 K along the cut illustrated in the inset. The overlaid plot represents the dispersion of the β band from fitting the MDCs. (b) Dispersion of the β band in panel (a) (circles), along with the assumed bare band dispersion and fitted Fermi velocity v_F^0 (solid line), and the renormalized low-energy dispersion with fitted v_F (dashed line). (c) MDCs of the spectra in panel (a). The blue, red, and green MDCs represent energies of E_F, $E_F - 75$ meV, and $E_F - 150$ meV, respectively. (d) Real part of the self-energy, ReΣ (red dots and curve), from the difference between the extracted dispersion and assumed bare band. (e) Imaginary part of the self-energy, ImΣ, estimated from the FWHM of the MDCs. The Kramers–Kronig transformation of ImΣ is plotted in panel (d) (black curve) for comparison with ReΣ.

coupling is likely responsible for the 75 meV kink in LiV_2O_4. Future phonon measurements or calculations on LiV_2O_4 considering the experimental flat band would be invaluable for quantifying the phononic contributions.

Regarding the origin of the 150 meV kink, neutron scattering experiments found no spin-related excitation modes near this energy.[29] The highest-energy phonon modes in $LiTi_2O_4$ are below 100 meV.[30] Given that high-energy vibrational modes in both LiV_2O_4 and $LiTi_2O_4$ primarily originate from O atom vibrations, phonon modes above 100 meV are not expected in LiV_2O_4.[31] Thus, we rule out the possibility that the 150 meV kink originates from electron coupling with a single bosonic quasiparticle. Notably, DMFT calculations reveal an incoherent a_{1g} spectral weight that approaches β at approximately 150 meV below the Fermi level [Fig. 2(g)], which may influence the dispersion and MDC peak width of the β band. Alternatively, the observed step-like structure of the imaginary part may suggest two-phonon scattering. Specifically, the self-energy exhibits a 68 meV increase from the Fermi level to the first plateau, followed by an additional 34 meV increase to a second plateau [Fig. 3(e)]. The relative magnitude is consistent with previous theoretical studies on weakly polar semiconductors, where two-phonon scattering, despite being a higher-order process, can have comparable strength to one-phonon scattering due to richer scattering channels.[32] In particular, the phonon at 75 meV in $LiTi_2O_4$ corresponds to a longitudinal optical mode, which is known to enable higher-order processes,[33,34] as evidenced in FeSe/$SrTiO_3$ heterostructures.[35] A similar mechanism may also be operative in LiV_2O_4, where multiphonon interactions involving longitudinal optical modes could give rise to the 150 meV kink.

In typical f-electron heavy-fermion systems like $CeCoIn_5$, ARPES measurements have shown that the quasiparticle spectral weight of the flat Ce 4f band near the Fermi level increases logarithmically with decreasing temperature, without saturation down to 17 K.[36] As the hybridization between the flat f-electron band and the dispersive conduction band strengthens, the Fermi momentum k_F varies with temperature, leading to a gradual reconstruction of the Fermi surface.[36] To examine whether similar phenomena occur in a 3d-electron heavy fermion system, we performed temperature-dependent ARPES measurements to track the evolution of the flat band in LiV_2O_4. As temperature decreases, the flat band of LiV_2O_4 becomes increasingly prominent [Figs. 4(a)–4(g)]. In the momentum-integrated EDCs, the flat band peak sharpens at lower temperatures, indicating enhanced coherence. However, the spectral weight of this peak spans a broad energy range exceeding 50 meV, far larger than the energy scale of heavy quasiparticles expected from $k_B T^* \approx 2.6$ meV. In contrast to $CeCoIn_5$, the flat band weight of α in LiV_2O_4 does not follow a logarithmic temperature dependence [Fig. 4(i)]. Instead, the flat band intensity is already present at 100 K and gradually saturates below 50 K, exhibiting no obvious correlation with the crossover temperature $T^* \approx 30$ K. This saturation may reflect the completion of orbital screening characteristic of Hund's metals, which can take place at a much higher temperature than the screening of spins.[37] Furthermore, as shown in Fig. 4(j), both the width and position of the MDC peaks at the Fermi level are nearly temperature-independent, in contrast to the c–f hybridization in $CeCoIn_5$, indicating stable orbital occupancy of the a_{1g} states. Consistently, orbital-selective nuclear magnetic resonance (NMR) measurements have suggested minimal temperature dependence in orbital populations.[38] The saturation of flat band intensity above 50 K and the lack of temperature-driven k_F variation distinguish the emergence of flat band in LiV_2O_4 from c–f hybridization in typical heavy-fermion systems. While the flat band in LiV_2O_4

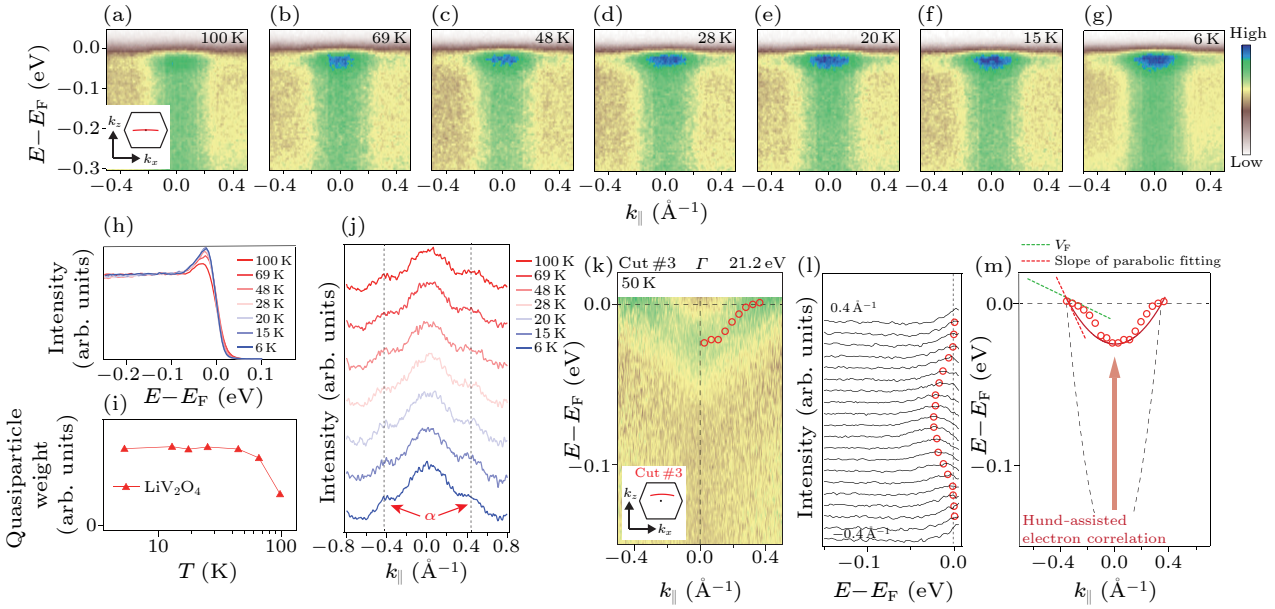

Fig. 4. (a)–(g) Temperature-dependent photoemission spectra along the Γ–M direction collected with 101 eV photons. The measurements were performed using linearly horizontal (LH) polarized photons. (h) Temperature-dependent EDCs integrated over the momentum window [−0.2 Å^{-1}, 0.2 Å^{-1}] around the Γ point. (i) Flat band weight of LiV_2O_4 obtained by integrating the spectral weight of the EDCs over the window of [E_F − 0.05 eV, E_F + 0.05 eV]. The procedure for extracting the flat band weight are explained in Section V of the SM. (j) MDCs integrated over $E_F \pm 5$ meV for the data in panel (a)–(g). The red arrows indicate the Fermi crossings of α band. (k) Photoemission spectra of cut #3 illustrated in the inset. The data were taken by He lamp ($h\nu = 21.2$ eV) at 50 K and divided by resolution-convolved Fermi Dirac Function. (l) EDCs from −0.4 Å^{-1} to 0.4 Å^{-1} for the data in panel (k). The red open circles were determined by the local maxima or shoulders. (m) Parabolic fitting of the α band dispersion and linear fitting to extract the Fermi velocity v_F, along with a schematic illustration of Hund-assisted electron correlations and additional many-body renormalization effects on the few-meV energy scale.

reflects strong correlations, the additional formation of heavy quasiparticles associated with this flat band likely occurs at a much lower energy scales below T^*.

An electron-like dispersion of the α band, with a bandwidth of approximately 25 meV, is resolved near E_F [Figs. 4(k) and 4(l), and Section Ⅲ of the SM]. This bandwidth is strongly renormalized compared to the corresponding DFT prediction [Fig. 2(g)]. Such a flat band is missing in previous angle-integrated photoemission spectroscopy studies,[10] possibly due to potential surface or crystal quality issues, a situation similar to early studies on $CeCu_2Si_2$.[39,40] Using the band bottom and Fermi crossing points, a parabolic estimation gives an effective mass of approximately $19m_e$ [Fig. 4(m)], which reflects the renormalization of the entire bandwidth by Hund-assisted electron correlation. However, closer to the Fermi level, the band dispersion is noticeably flatter, deviating from a simple parabolic dispersion. This feature is consistently observed at various temperatures (Section Ⅳ of the SM) and signals additional renormalization on a few-meV energy scale. The Fermi velocity is estimated to be $v_F = 0.034$ eV·Å, which is 3% of that of the β band. By comparing the v_F with the slope of parabolic estimation at E_F, the additional renormalization further enhances the effective mass to at least $93m_e$. This few-meV renormalization scale is consistent with the expected energy scale of heavy quasiparticles ($k_BT^* \approx 2.6$ meV), and the enhanced effective mass is comparable to the value of $180m_e$ inferred from specific heat measurements.[12] The remaining discrepancy, approximately a factor of 2, likely arises from the continued development of low-energy renormalization at lower temperatures and the limited energy resolution of our measurements, which may not fully capture the small energy scale involved. An accurate determination of the effective mass and full characterization of the quasiparticle dispersion will require sub-meV energy resolution at temperatures below 2 K, when the heavy Fermi liquid state is fully developed.[19]

3. Discussions. The entire bandwidth of α is substantially renormalized with respect to DFT calculations [Fig. 2(g)]. Such bandwidth narrowing and mass enhancement are characteristic of strong electron correlations and are commonly observed in systems near Mott transitions. For example, in $NiS_{2-x}Se_x$, increasing correlation strength gradually reduces the bandwidth as the system approaches the Mott transition.[41] Analogously, in LiV_2O_4, the strong correlations within the a_{1g} orbital may push it close to an orbital-selective Mott–Hubbard transition. Although the coherent weight of the α band does not correspond to the Kondo screening in typical heavy fermion systems, its saturation may reflect the full screening of orbital degrees of freedom, as expected in the Hund's metal scenario.[37] The well developed coherent dispersion of α band establishes the prerequisite for the formation of lower-energy heavy quasiparticles.

The additional renormalization at E_F suggests coupling with excitations on the few-meV energy scale. NMR studies indicate antiferromagnetic correlations between V

atoms,[38] while inelastic neutron scattering experiments have detected short-range spin fluctuations with characteristic energies from 0.2 to 0.8 meV.[29] In the geometrically frustrated pyrochlore sublattice formed by V atoms, such low-energy spin excitations are expected to remain dynamic and can couple to electrons near the Fermi level. This coupling may have induced the observed additional renormalization on a few-meV energy scales, enhancing the effective mass beyond the renormalization of the entire bandwidth by electron-electron interactions and Hund's coupling.

In summary, our study provides the first direct observation of the three-dimensional electronic structure of LiV_2O_4. We identify a flat, heavy α band associated with the a_{1g} orbital, whose strong mass renormalization arises from cooperative effects of Hund's coupling and electronic correlations. Furthermore, we uncover higher-order electron–boson coupling in the itinerant β band, revealing further many-body interactions that should be incorporated into theoretical models. In addition to the renormalization of the a_{1g} orbital over the entire bandwidth, possible low-energy interactions with excitations induced by geometric frustration contribute to the exceptionally large effective mass inferred from thermodynamic measurements. These findings advance our understanding of heavy fermion physics in 3d transition-metal systems and lay the groundwork for future exploration of exotic quantum phases in correlated oxides.

Note. During the revision of our manuscript, we became aware of the preprint of an independent study by Dongjin Oh, *et al.*,[42] which also reported measurements of the three-dimensional electronic structure and flat band of LiV_2O_4.

Acknowledgements. We gratefully acknowledge the valuable discussion with Dr. P. Y. Zheng, Dr. Z. H. Yuan, and Dr. Y. L. Wang, the experimental support of Dr. Z. T. Liu, Dr. Z. C. Jiang, Dr. Marta Zonno, and Dr. Sergey Gorovikov. This work was supported in part by the National Key R&D Program of the MOST of China (Grant No. 2023YFA1406300), the National Natural Science Foundation of China (Grant Nos. 12274085, 12422404, and 92477206), the New Cornerstone Science Foundation, the Innovation Program for Quantum Science and Technology (Grant No. 2021ZD0302803), and Shanghai Municipal Science and Technology Major Project (Grant No. 2019SHZDZX01). The ARPES measurements used Beamlines 09U and 03U of the SSRF and Beamline QMSC of Canadian Light source. The Beamline 03U is supported by the ME2 project from the National Natural Science Foundation of China (Contract No. 11227902).

References

[1] White B, Thompson J, and Maple M 2015 *Physica C* **514** 246
[2] Stewart G R 2017 *Adv. Phys.* **66** 75
[3] Machida K, Ozaki M, and Ohmi T 1989 *J. Phys. Soc. Jpn.* **58** 4116
[4] Stewart G R 1984 *Rev. Mod. Phys.* **56** 755
[5] Bauer E, Hilscher G, Michor H, Paul C, Scheidt EW, Gribanov A, Seropegin Y, Noël H, Sigrist M, and Rogl P 2004 *Phys. Rev. Lett.* **92** 027003
[6] Schröder A, Aeppli G, Coldea R, Adams M, Stockert O, Löhneysen H, Bucher E, Ramazashvili R, and Coleman P 2000 *Nature* **407** 351
[7] Allan M P, Massee F, Morr D, Van Dyke J, Rost A W, Mackenzie A, Petrovic C, and Davis J C 2013 *Nat. Phys.* **9** 468
[8] Steglich F, Aarts J, Bredl C D, LiekeW, Meschede D, FranzW, and Schäfer H 1979 *Phys. Rev. Lett.* **43** 1892
[9] Fulde P, Keller J, and Zwicknagl G 1988 *Solid State Physics* **4** 1
[10] Shimoyamada A, Tsuda S, Ishizaka K *et al.* 2006 *Phys. Rev. Lett.* **96** 026403
[11] Kondo S, Johnston D, Swenson C *et al.* 1997 *Phys. Rev. Lett.* **78** 3729
[12] Johnston D C 2000 *Physica B* **281** 21
[13] Anisimov V, Korotin M, Zölfl M, Pruschke T, Le Hur K, and Rice T 1999 *Phys. Rev. Lett.* **83** 364
[14] Nekrasov I A, Pchelkina Z, Keller G, Pruschke T, Held K, Krimmel A, Vollhardt D, and Anisimov V 2003 *Phys. Rev. B* **67** 085111
[15] Arita R, Held K, Lukoyanov A, and Anisimov V 2007 *Phys. Rev. Lett.* **98** 166402
[16] Grundner M, Kugler F B, Parcollet O, Schollwöck U, Georges A, and Hampel A 2025 *Phys. Rev. B* **112** L041106
[17] Knox K, Abeykoon A, Zheng H, Yin W, Tsvelik A, Mitchell J, Billinge S, and Bozin E 2013 *Phys. Rev. B* **88** 174114
[18] Lee J, Ma J, Hahn S, Cao H, Lee M, Hong T, Lee H, Yeom M, Okamoto S, and Zhou H 2017 *Sci. Rep.* **7** 17129
[19] Urano C, Nohara M, Kondo S, Sakai F, Takagi H, Shiraki T, and Okubo T 2000 *Phys. Rev. Lett.* **85** 1052
[20] Jönsson P, Takenaka K, Niitaka S, Sasagawa T, Sugai S, and Takagi H 2007 *Phys. Rev. Lett.* **99** 167402
[21] Matsushita Y, Ueda H, and Ueda Y 2005 *Nat. Mater.* **4** 845
[22] Niemann U, Wu Y M, Oka R, Hirai D, Wang Y, Suyolcu Y E, Kim M, van Aken P A, and Takagi H 2023 *Proc. Natl. Acad. Sci. U.S.A.* **120** e2215722120
[23] Yajima T, Soma T, Yoshimatsu K, Kurita N, Watanabe M, and Ohtomo A 2021 *Phys. Rev. B* **104** 245104
[24] Backes S, Nomura Y, Arita R, and Shinaoka H 2025 *Phys. Rev. B* **111** L041102
[25] Tang C, Lin Z, Zhang J *et al.* 2022 *npj Quantum Mater.* **7** 53
[26] Hofmann P, Sklyadneva I Y, Rienks E, and Chulkov E V 2009 *New J. Phys.* **11** 125005
[27] Sushkov A B, Tchernyshyov O, II W R, Cheong S W, and Drew H D 2005 *Phys. Rev. Lett.* **94** 137202
[28] Lutz H, Müller B, and Steiner H 1991 *J. Solid State Chem.* **90** 54
[29] Lee S H, Qiu Y, Broholm C, Ueda Y, and Rush J J 2001 *Phys. Rev. Lett.* **86** 5554
[30] He G, Jia Y, Hou X *et al.* 2017 *Phys. Rev. B* **95** 054510
[31] Ashcroft N W and Mermin N 1976 *Solid state physics* (Cengage Learning)
[32] Lee N E, Zhou J J, Chen H Y, and Bernardi M 2020 *Nat. Commun.* **11** 1607
[33] Fröhlich H 1954 *Adv. Phys.* **3** 325
[34] Vogl P 1976 *Phys. Rev. B* **13** 694
[35] Liu C, Day R P, Li F *et al.* 2021 *Nat. Commun.* **12** 4573
[36] Chen Q Y, Xu D F, Niu X H, Jiang J, Peng R, Xu H C, Wen C H P, Ding Z F, Huang K, Shu L, Zhang Y J, Lee H, Strocov V N, Shi M, Bisti F, Schmitt T, Huang Y B, Dudin P, Lai X C, Kirchner S, Yuan H Q, and Feng D L 2017 *Phys. Rev. B* **96** 045107
[37] Deng X, Stadler K M, Haule K, Weichselbaum A, von Delft J, and Kotliar G 2019 *Nat. Commun.* **10** 2721
[38] Shimizu Y, Takeda H, Tanaka M, Itoh M, Niitaka S, and Takagi H 2012 *Nat. Commun.* **3** 981

[39] Reinert F, Ehm D, Schmidt S, Nicolay G, Hüfner S, Kroha J, Trovarelli O, and Geibel C 2001 *Phys. Rev. Lett.* **87** 106401
[40] Wu Z, Fang Y, Su H *et al.* 2021 *Phys. Rev. Lett.* **127** 067002
[41] Xu H C, Zhang Y, Xu M, Peng R, Shen X P, Strocov V N, Shi M, Kobayashi M, Schmitt T, Xie B P, and Feng D L 2014 *Phys. Rev. Lett.* **112** 087603
[42] Oh D, Hampel A, Wakefield J P, Moen P, Smit S, Luo X, Zonno M, Gorovikov S, Leandersson M, Polley C, Kundu A K, Rajapitamahuni A, Vescovo E, Jozwiak C, Bostwick A, Rotenberg E, Isobe M, Verma M, Crispino M, Grundner M, Kugler F B, Parcollet O, Schollwöck U, Takagi H, Damascelli A, Sangiovanni G, Checkelsky J G, Georges A, and Comin R 2025 arXiv:2502.07234 [cond-mat.str-el]